



Temperature (208-318 K) and pressure (18-696 Torr) dependent rate coefficients for the reaction between OH and HNO₃.

Katrin Dulitz^{1,a}, Damien Amedro¹, Terry J. Dillon^{1,b}, Andrea Pozzer¹, and John N Crowley¹

¹ Division of Atmospheric Chemistry, Max-Planck-Institut für Chemie, 55128 Mainz, Germany

^a now at: Nanophysics research group, University of Freiburg, 79104 Freiburg, Germany

^b now at: Department of Chemistry, University of York, York, U.K

Correspondence to: John Crowley (john.crowley@mpic.de)

Abstract. Rate coefficients (k_5) for the title reaction were obtained using pulsed laser photolytic generation of OH coupled to its detection by laser-induced fluorescence (PLP-LIF). More than eighty determinations of k_5 were carried out in nitrogen or air bath gas at various temperatures and pressures. The accuracy of the rate coefficients obtained was enhanced by in-situ measurement of the concentrations of both HNO₃ reactant and NO₂ impurity. The rate coefficients show both temperature and pressure dependence with a rapid increase in k_5 at low temperatures. The pressure dependence was weak at room temperature but increased significantly at low temperatures. The entire dataset was combined with selected literature values of k_5 and parameterised using a combination of pressure dependent and independent terms to give an expression that covers the relevant pressure and temperature range for the atmosphere. A global model, using the new parameterisation for k_5 rather than those presently accepted, indicated small but significant latitude and altitude dependent changes in the HNO₃ / NO_x ratio of between -6% and +6%. Effective HNO₃ absorption cross sections (184.95 and 213.86 nm, units of cm² molecule⁻¹) were obtained as part of this work: $\sigma_{213.86} = 4.52^{+0.23}_{-0.12} \times 10^{-19}$ and $\sigma_{184.95} = 1.61^{+0.08}_{-0.04} \times 10^{-17}$.

1 Introduction

Nitric acid, ubiquitous to the Earth's atmosphere, is formed mainly in the association reaction between nitrogen dioxide and hydroxyl radicals (R1) and is an important reservoir species for NO_x (where NO_x is defined as the sum of NO and NO₂), especially at higher altitudes, e.g. in the lower stratosphere where it represents ~ 80-100% of reactive nitrogen oxides (NO_y = NO_x + HNO₃ + PAN + 2N₂O₅ etc.). Recent laboratory studies (Butkovskaya et al., 2007; Butkovskaya et al., 2009) suggest that HNO₃ may also be formed (at < 1% yield) in the reaction of HO₂ with NO, which can double the HNO₃ production rate in e.g. the tropical tropopause (R2) (Cariolle et al., 2008). The reaction of nitrate radicals (NO₃) with some organic trace gases (RH) including aldehydes and dimethylsulphide can be a significant direct source of HNO₃ at night (R3), as can the heterogeneous hydrolysis of both N₂O₅ and organic nitrates, RONO₂, (R4) in conjunction with gas-liquid partitioning. As NO₃, N₂O₅ and RONO₂ are all formed in the atmosphere via oxidation of NO and NO₂, these processes indirectly convert NO_x to HNO₃.



5 Reaction with the hydroxyl radicals (OH, R5) and photolysis (R6) are the major gas-phase HNO_3 loss processes:



which result in atmospheric lifetimes of several weeks in the troposphere and lower stratosphere. Due to its high solubility, wet and dry deposition reduce the lifetime of HNO_3 in the planetary boundary layer to a few days. The nitrate radical product
10 of R5 (NO_3) is rapidly converted to either NO_2 and NO by photolysis or to NO_2 by reaction with NO , so that (R5) represents an important route for re-activation of NO_x from the long-lived HNO_3 reservoir. Traditionally, atmospheric models have tended to over-predict nitric acid concentrations and under-predict NO_x to HNO_3 ratios, with the largest discrepancy found at high altitudes. The model-measurement discrepancy may be related to unknown (or more rapid) re-noxification processes, either gas-phase or heterogeneous (see e.g. Thakur et al. (1999) and Schultz et al. (2000) and references therein for a
15 summary) or due to difficulties in modelling NO_x input from lightning and HNO_3 scavenging (Staudt et al., 2003). Given the major role of HNO_3 re-noxification in determining e.g. O_3 production rates in the atmosphere, it is of major importance to reduce the uncertainty in the rate coefficient for the title reaction.

The important atmospheric role of the reaction between OH and HNO_3 is reflected in the numerous experimental determinations of the rate coefficient (k_5) and the products as listed and reviewed by evaluation panels (Atkinson et al., 2004;
20 Sander et al., 2006). Most of the experimental studies were carried out in the mid-70s to mid-80s (Margitan et al., 1975; Smith and Zellner, 1975; Wine et al., 1981; Jourdain et al., 1982; Kurylo et al., 1982; Margitan and Watson, 1982; Marinelli and Johnston, 1982; Ravishankara et al., 1982; Devolder et al., 1984; Smith et al., 1984; Connell and Howard, 1985; Jolly et al., 1985; Stachnik et al., 1986) with only the most recent and comprehensive studies of the reaction (Brown et al., 1999; Brown et al., 2001) extending the temperature range to those found at the tropopause. Experimental (Carl et al., 2001;
25 McCabe et al., 2003; O'Donnell et al., 2008b) and theoretical (Xia and Lin, 2001; Gonzalez and Anglada, 2010) work examining the details of the reaction mechanism highlight continuing interest in this complex reaction, which proceeds via formation of a pre-reaction complex, HO- HNO_3 (Aloisio and Francisco, 1999; Brown et al., 1999; Brown et al., 2001; Xia and Lin, 2001; O'Donnell et al., 2008a). HO- HNO_3 can (a) dissociate into reactants, (b) rearrange to form products via a transition state which lies somewhat higher in energy than the reactants or (c) experience collisional deactivation by bath gas
30 molecules. Dissociation of the thermalised complex into the NO_3 and H_2O reaction products is via tunnelling through the exit barrier, which explains the unusual kinetics observed, with k_5 increasing with pressure and decreasing temperature (Margitan and Watson, 1982; Stachnik et al., 1986; Brown et al., 1999). No evidence for products apart from NO_3 and H_2O has been obtained (Atkinson et al., 2004).



As mentioned above, prior to the present dataset, only Brown et al. (1999) had conducted experiments under conditions of temperature and pressure relevant for the tropopause / lower stratosphere (< 240 K). The experiments of Brown et al. revealed a rapid increase in k_5 at low temperatures, leading to a reduced NO_2 to HNO_3 ratio in models of this part of the atmosphere. The important findings of Brown et al. require confirmation from independent experiments and the present study is intended to provide highly accurate rate coefficients which cover sufficient parameter space to do this.

2 Experimental

2.1 Pulsed laser photolysis, laser induced fluorescence set-up

Rate coefficients (k_5) for the title reaction were determined using pulsed laser photolysis (PLP) coupled to laser-induced fluorescence detection (LIF) as illustrated in Fig. 1. A detailed description of the PLP-LIF apparatus has been published (Wollenhaupt et al., 2000) and only essential details and modifications are reproduced here. The central component is a quartz reactor, the temperature of which was controlled by circulating a cryogenic fluid through an outer jacket. The inner wall of the reactor was coated with a thin film of Teflon (DuPont, FEP TE9568) to reduce adsorption of HNO_3 . The temperature at the intersection of the laser beams (defining the reaction volume) was monitored by a thermocouple before and after each experimental series. All kinetic measurements were carried out under “slow flow conditions” with approximate linear flow velocities of 10 cm s^{-1} preventing the build-up of reaction products inside the reaction volume. The reactor pressure was monitored using calibrated 100 Torr and 1000 Torr capacitance manometers.

2.2 Generation and detection of OH

A KrF exciplex laser (Lambda Physik Lextra 50), operated at $\lambda = 248 \text{ nm}$, was used to produce OH radicals from HNO_3 which served both as reactant and precursor (R6). Hydroxyl radicals were excited by a Nd-YAG pumped dye laser (rhodamine 6G, Lambda Physik Scanmate) at $\lambda = 281.915 \text{ nm}$ ($\text{A}^2\Sigma^+ (v' = 1) \leftarrow \text{X}^2\Pi(v'' = 0)$, $\text{Q}_1(1)$ transition). OH fluorescence from the electronic $\text{A}^2\Sigma^+ (v' = 0) \rightarrow \text{X}^2\Pi(v'' = 0)$ transition at $\lambda \approx 309 \text{ nm}$ was collected by a MgF_2 lens located perpendicular to the laser beams and detected by a photomultiplier tube (PMT) connected to a gated boxcar integrator. An interference filter ($309 \pm 5 \text{ nm}$) and a BG 26 glass cut-off filter were used to decrease scattered light at the PMT. The exciplex laser fluence was measured by a calibrated Joule meter located at the end of the beam axis in order to estimate OH concentrations, $[\text{OH}]$. The exciplex laser fluence was adjusted so that the $[\text{HNO}_3]/[\text{OH}]$ ratio was always $> 10^4$ ensuring first-order conditions and suppressing interfering secondary OH chemistry (see section 3.3).

2.3 HNO_3 flows and concentration measurement

Frequently, in a study of this sort where pseudo-first order kinetics are anticipated, the main source of error in deriving the rate constant is the measurement of the concentration of the excess reagent (HNO_3 in this case) and any impurities that may



also react with OH. For this reason, much effort was dedicated to the accurate, in-situ measurement of HNO₃ concentrations using spectroscopic methods and also optical detection (and reduction) of potential impurities.

Gas-phase HNO₃ was eluted into the reactor in a flow of N₂ which was passed over a liquid HNO₃ reservoir prior to mixing and dilution with bath gas. Three different liquid HNO₃ sources were used: a ternary mixture (50 wt.% HNO₃ / 22 wt.% H₂SO₄), anhydrous HNO₃, and 90% HNO₃. The ternary mixture was used only in experiments at $T > 263$ K due to HNO₃ condensation inside the photolysis reactor at lower temperatures. The anhydrous HNO₃ sample was found to contain traces of NO₃ as observed previously (Crowley et al., 1993). These could be significantly reduced by the addition of H₂O to generate the 90 wt.% sample.

2.3.1 HNO₃ concentration measurement using absorption spectroscopy

Nitric acid concentrations were determined optically using dual beam absorption cells located downstream of the photolysis reactor. The first absorption cell ($l = 43.8$ nm) was equipped with a low pressure, Hg “Penray” lamp to measure the attenuation of light by HNO₃ at 184.95 nm (Wollenhaupt et al., 2000) and was used mainly at $T \leq 227$ K where low HNO₃ concentrations were used. For experiments above 227 K, HNO₃ absorption at 213.86 nm in the second optical absorption cell ($l = 34.8$ cm) equipped with a low-pressure zinc lamp (213.86 nm) and (214 ± 10) nm bandpass filter (LOT-Oriel) was used to determine [HNO₃]. For the 184.95 nm measurements the transmitted light intensity was corrected for detection of “wrong” wavelengths (e.g. 253.65 nm) by adding large concentrations of gases (N₂O or CCl₄) which attenuate the 184.95 line completely. This method of measurement of nitric acid effectively integrates its concentration throughout the reactor and, if wall losses of HNO₃ result in significant radial gradients in its concentration, may not necessarily give a representative measure of [HNO₃] at the centre of the reactor, especially when the reactor was cold. For this reason, we also measured the HNO₃ concentration the centre of the reactor (in the same volume in which OH decays were recorded) using a two-photon excitation scheme which is summarised briefly below.

2.3.2 HNO₃ Concentration Measurement via two-photon excitation at 193 nm

The detection of HNO₃ via two-photon excitation at 193 nm (Two Photon, Excited Fragment Spectroscopy, TPEFS) was pioneered by Stuhl and co-workers and used to measure HNO₃ in ambient air (Papenbrock et al., 1984; Kenner et al., 1985; Kenner et al., 1986; Papenbrock and Stuhl, 1991) We shall present a detailed description of the detection scheme and the photo-physics involved and the application of TPEFS to kinetic studies in a separate publication and simply outline the central features here. HNO₃ is converted in a sequential, two-photon process to an electronically excited hydroxyl radical, OH(A), the fluorescence of which can be detected at 308 nm. Excited (triplet state) HONO is believed to be formed upon absorption of the first 193 nm photon and dissociated to OH(A) and NO(X,A) by the second photon. Gently focussing the 193 nm beam from an ArF Excimer laser to a diameter of about 1 mm was sufficient to obtain a detection limit of $\approx 10^8$ molecule cm⁻³ at 50 Torr of N₂ bath gas.



The TPEFS detection of HNO₃ was calibrated by flowing pure samples of HNO₃ through the reactor, and monitoring its concentration by absorption spectroscopy at 184.95 nm.

2.4 On-line Determination of Nitrogen Dioxide Concentrations

A major potential systematic error in measuring the rate coefficient for OH + HNO₃ is the presence of NO₂, an unavoidable impurity in HNO₃ samples, which reacts rapidly with OH, especially at high pressures and low temperatures. NO₂ is formed in the heterogeneous decomposition of gaseous HNO₃ on surfaces and, to a lesser extent, due to the liquid-phase disproportionation of anhydrous HNO₃ and thermal decomposition of N₂O₅ (R7 and R8) (Crowley et al., 1993).



NO₂ impurity levels were measured in-situ using a multi-pass absorption cell ($l = 880$ cm) positioned downstream of the LIF reactor and the other optical cells. Light from a halogen lamp passing through the cell was focused onto the entrance slit of a 0.5 m monochromator (B&M Spektronik BM50, 600 lines mm⁻¹ grating blazed at 500 nm). A diode-array detector (Oriel Instaspec 2) was used to record NO₂ absorption between 398 and 480 nm. The instrumental resolution ($\delta\lambda = 0.32$ nm) was determined from the full width at half maximum (FWHM) of the 435.8 nm Hg emission line.

2.5 Determination of NO, NO₃ and HONO impurities

The same multi-pass absorption cell was used to monitor NO₃ (592-671 nm) and HONO (253-335 nm) impurities. NO concentrations were estimated using a 30.4 cm absorption cell with a D₂ lamp providing analysis light between 177 and 260 nm. For this measurement, the monochromator (600 lines mm⁻¹ grating blazed at 200 nm) was purged with nitrogen. The instrumental resolution was set at 0.32 nm (FWHM of a Hg line) in every experiment.

2.6 HNO₃ Absorption Cross Sections at 213.86 nm and 184.95 nm

The 213.86 nm optical absorption setup was used to determine an effective HNO₃ absorption cross section at this wavelength. In these experiments, a flow of undiluted, anhydrous nitric acid was passed through the 34.8 cm absorption cell with concentrations calculated from the HNO₃ pressure, which was measured with a 2 Torr capacitance manometer. The accuracy of the pressure measurement was confirmed by cross-checking with 0.1 Torr and 10 Torr manometers. The temperature of the cell was monitored with a thermocouple. Light intensity in the absence of HNO₃ was obtained by evacuating the absorption cell and purging with N₂. An absorption cross section at 184.95 nm was derived by connecting the 184.95 and 213.86 nm optical absorption cells in series and measuring relative optical densities at both wavelengths for the same sample.



2.7 Chemicals

Anhydrous nitric acid was prepared by mixing KNO_3 (Merck) with H_2SO_4 (95-98 wt.%, Roth) and condensing the HNO_3 vapour into a liquid nitrogen trap. The ternary mixture (50 wt.% HNO_3 / 22 wt.% H_2SO_4) was made from H_2SO_4 (95-98 wt.%, Roth) and HNO_3 (65 wt.%, Roth). All nitric acid sources were stored at $T = 253$ K between experiments. Apart from
5 experiments in N_2 bath gas (Westfalen, 5.0) a few measurements were conducted in air (approx. 79% N_2 , 21% O_2) by mixing N_2 carrier gas with O_2 (Air Liquide, 4.5).

3 Results and Discussion

3.1 HNO_3 Absorption Cross Sections at 213.86 nm and 184.95 nm

The HNO_3 absorption cross section at 213.86 nm, $\sigma_{213.86 \text{ nm}}$, was determined by measuring optical density while varying the
10 HNO_3 pressure between 0.125 Torr and 2.019 Torr. HNO_3 concentrations were varied either by adjusting the valves at the entrance or at the exit of the absorption cell or by increasing the temperature of the HNO_3 reservoir, both methods giving the same result. The cross section determinations are summarised in Fig. 2 where measured optical densities at 213.86 nm ($\text{OD}_{213.86}$) are related to the HNO_3 concentration and the cross section, $\sigma_{213.86}$, via the Beer-Lambert expression:

$$\text{OD}_{213.86} = \ln\left(\frac{I_0}{I}\right) = \sigma_{213.86 \text{ nm}} \cdot l \cdot [\text{HNO}_3] \quad (\text{i})$$

15 where l is the cell length (34.8 cm) and I_0 and I are the intensities of incident and transmitted light at 213.86 nm, respectively. A linear regression yields a value of $\sigma_{213.86 \text{ nm}} = 4.52 \times 10^{-19} \text{ cm}^2 \text{ molecule}^{-1}$, whereas a proportional fit yields $\sigma_{213.86 \text{ nm}} = 4.59 \times 10^{-19} \text{ cm}^2 \text{ molecule}^{-1}$ (both at 300 K). The small difference (less than 1.5%) is caused by an offset of 0.01 in optical density, which may be due to HNO_3 adsorbed on optical windows of the absorption cell. The total uncertainty in $\sigma_{213.86}$ was assessed by considering the difference in cross section obtained from the linear and proportional fits, the
20 estimated error in cell length ($\Delta l = 0.1$ cm) and the statistical error (0.1%) from the linear fit. In addition, the contribution from impurities N_2O_5 (0.2%), NO_2 (0.2%), NO_3 (0.01%) and H_2O (2%) was found to contribute a lower limit of 1.2% and an upper limit of 2.0% to the error estimate for $\sigma_{213.86 \text{ nm}}$. The final result is thus $\sigma_{213.86 \text{ nm}} = 4.52_{-0.12}^{+0.23} \times 10^{-19} \text{ cm}^2 \text{ molecule}^{-1}$.

An effective HNO_3 cross section at 184.95 nm, $\sigma_{184.95 \text{ nm}}$, was obtained by measuring the optical densities in both absorption cells simultaneously. The different cell lengths and small differences in the pressure and temperature between the cells were
25 accounted for in calculating $[\text{HNO}_3]$. As can be seen from the inset in Fig. 2, a linear relationship was observed, which resulted in an HNO_3 absorption cross section (at 300 K) of $\sigma_{184.95 \text{ nm}} = 1.61_{-0.04}^{+0.08} \times 10^{-17} \text{ cm}^2 \text{ molecule}^{-1}$. As the relative cross section is very accurately defined, the errors in the cross section at 184.95 nm stem almost entirely from those in the absolute value at 213.86 nm. HNO_3 cross sections at these wavelengths have been previously reported. Brown et al. (1999) quote a 213.86 nm absorption cross section of $(4.52 \pm 0.19) \times 10^{-19} \text{ cm}^2 \text{ molecule}^{-1}$, obtained by interpolating the HNO_3 absorption



spectrum of Burkholder et al. (1993) This value agrees well with that obtained in the present experiment. A very similar value of $\sigma_{183.95 \text{ nm}} = 1.63 \times 10^{-17} \text{ cm}^2 \text{ molecule}^{-1}$ was first determined by (Biaume, 1973-1974) and confirmed by Wine et al. (1981) and Connell and Howard (1985) The excellent agreement with previous results indicates that our absorption cross sections are well-suited for the in-situ optical determination of HNO_3 concentrations.

5 3.2 HNO_3 Detection using two-photon excitation at 193 nm

The measurement of the HNO_3 concentration downstream of the vessel in which the reaction takes place may lead to a systematic bias in the rate constant if HNO_3 is partitioned significantly to surfaces. Uptake of HNO_3 to the reactor wall will result in radial gradients in the reactor, especially at high pressures where mixing by radial diffusion is slow. Similar to the study of Brown et al. (1999) we observed significant loss of HNO_3 from the gas-phase at low temperatures, presumably the result of condensation on the cold reactor walls. We would then expect that the HNO_3 concentration close to the walls is lower than that in the centre of the reactor, implying that any method of HNO_3 concentration measurement that integrates over the entire reactor diameter will generate rate constants that are too high at low temperatures. This applies equally to the present study, where HNO_3 is measured downstream after turbulent mixing of gas leaving the reactor and also to the experiments of Brown et al. (1999) who monitored the HNO_3 concentration across the diameter of the reaction vessel as well as downstream in a separate optical absorption cell.

We used the TPEFS technique outlined in Section 2.3 to measure the HNO_3 concentration in the centre of the reactor where OH was measured in the kinetic experiments and compared it with that measured in online absorption cells (184.9 and 213.9 nm) located downstream of the reactor. For consistency, we used similar flows, pressures and HNO_3 concentrations to those used for determining k_5 . In order to simplify the analysis, most of the experiments were conducted at constant gas densities and $[\text{HNO}_3]$. In some experiments where the nitric acid concentrations could not be kept constant (mainly at low temperature and high $[\text{HNO}_3]$), we corrected the TPEFS signal for 193 nm light absorption and HNO_3 quenching of the OH fluorescence. Details of the corrections are provided in the supplementary information (Fig. S1-S3).

The TPEFS signal and HNO_3 concentration (184.95 nm absorption) were recorded at a high temperature and the reactor was subsequently cooled to the next (lower) temperature with the pressure adjusted to keep the same molecular density. In complementary experiments, the HNO_3 concentrations and densities were varied from 7.0×10^{13} to $3.0 \times 10^{16} \text{ molecule cm}^{-3}$ and 1.6×10^{18} to $4.4 \times 10^{18} \text{ molecule cm}^{-3}$, respectively. Figure 3 shows the normalised TPEFS signal as a function of temperature. The signal was normalised to the average $[\text{HNO}_3] / \text{TPEFS}$ ratio obtained at the temperatures above 0°C where effects of HNO_3 condensation were negligible. A ratio lower than unity thus indicates that use of the 184.95 nm optical absorption measurements to measure $[\text{HNO}_3]$ can result in an underestimation of the HNO_3 concentration in the middle of the reactor compared to the usual online measurement using the absorption cell downstream of the reactor. At the lowest temperatures ($T < 233 \text{ K}$), we observed some deviation ($10 \pm 10\%$ at 208 K), indicating a possible underestimation of the HNO_3 concentration, but within the uncertainty of the measurement. The increase in the uncertainty in TPEFS sensitivity at



low temperatures is related to experimental problems keeping HNO_3 constant at these temperatures: We conclude that the effects of HNO_3 concentration gradients are $< 10\%$ under our experimental conditions and add an additional 10% uncertainty for the kinetic measurements at temperatures below 240 K .

3.3 Impurities

5 As the reaction between NO_2 and OH (R1) is pressure and temperature dependent and the rate coefficients are considerably larger than for (R5), even small amounts of NO_2 can contribute significantly to the OH decay measured in a study of k_5 . Fortunately, NO_2 possesses a distinct, structured absorption spectrum with sufficiently large differential absorption cross sections to make accurate concentration measurements at low impurity levels possible. NO_2 optical densities over the 880 cm optical path length were measured online using a multi-pass cell located downstream of the photolysis reactor. NO_2 concentrations were calculated by least-squares fitting to a reference spectrum (Bogumil et al., 2003) (see Fig. 4). The limit of detection (LOD) was $[\text{NO}_2] \approx 2 \times 10^{11}\text{ molecule cm}^{-3}$. The NO_2 content depended upon the HNO_3 source used and was observed to decrease in the order anhydrous $\text{HNO}_3 >$ ternary mixture $> 90\% \text{ HNO}_3$. No difference in the $[\text{HNO}_3]/[\text{NO}_2]$ ratio was observed when the absorption cell was relocated upstream of the LIF reactor. In general, the NO_2 impurity levels were low, with an $\text{HNO}_3 / \text{NO}_2$ ratio $> 10^4$ so that NO_2 measurement was only possible at high HNO_3 concentrations, e.g., at room temperature. NO_2 is also generated as co-product in the photolysis of HNO_3 to make OH (R6). In this case the $[\text{HNO}_3]/[\text{OH}]$ ratio was usually also 10^4 , making this a comparable (and thus also negligible) source of NO_2 . Using literature rate coefficients (Atkinson et al., 2004; Sander et al., 2006) for the reaction between NO_2 and OH (1) a contribution of R1 to the OH loss rate could be calculated from each individual decay. This was always less than 1% of the total measured OH decay rate constant and less than 0.2% at low pressures ($p \leq 50\text{ Torr}$). The use of relatively low OH concentrations ($10^{11}\text{ molecule cm}^{-3}$) also makes the contribution of OH self-reactions ($k_{\text{OH}+\text{OH}} \approx 4 \times 10^{-12}\text{ cm}^3\text{ molecule}^{-1}\text{ s}^{-1}$ at 298 K and 200 Torr) (Atkinson et al., 2004) negligibly small.

Operating under conditions of low conversion of HNO_3 is important for reduction of the impact of rapid secondary reactions of OH with e.g. NO_3 (formed in R5) or with HO_2 (formed in the reaction of OH with NO_3). Although the OH decay rate can be significantly enhanced by secondary reactions when $[\text{HNO}_3]/[\text{OH}] \leq 1000$, for $[\text{HNO}_3]/[\text{OH}] > 10^4$ this is avoided. This highlights an important advantage of real-time (e.g. pulsed/flash photolysis) experiments on (R5) compared to flow tubes, which are restricted by issues of spatial resolution in the amount of HNO_3 that can be employed. The main advantage is however the possibility to explore a greater spread of temperatures and pressures and to work under essentially wall free conditions, which is important when dealing with OH and HNO_3 which both have high affinities for surfaces.

The multi-pass absorption cell was also used to check for NO_3 and HONO. Although NO_3 absorption was indeed observed with the anhydrous nitric acid source, the mixing ratio relative to HNO_3 was very low, i.e., $[\text{NO}_3]/[\text{HNO}_3] < 10^{-5}$. Through the addition of $\approx 10\% \text{ H}_2\text{O}$ (i.e. using the $90\% \text{ HNO}_3$ solution) the NO_3 concentration was further reduced by more than an order of magnitude. At these levels, NO_3 does not influence the OH decay rates by more than 0.1% . NO_3 absorption bands were not observed when using the ternary mixture.



We were unable to detect HONO or NO absorption features in any of the HNO₃ sources. Detection limits, were $\approx 5 \times 10^{13}$ molecule cm⁻³ for NO and $\approx 2 \times 10^{13}$ molecule cm⁻³ for HONO. At these levels, the impact on the OH decay rate or HNO₃ concentration measurement at 213.86 nm is negligible, e.g., an NO impurity level of $\approx 3\%$ would bias the quantitative HNO₃ absorption measurements at 213.86 nm by less than 2%.

5 3.4 Rate Coefficients (k_5) for HNO₃ + OH

All kinetic experiments were carried out under pseudo-first-order conditions, i.e. [HNO₃] \gg [OH] so that the OH decay can be described as follows:

$$\ln\left(\frac{[\text{OH}]_t}{[\text{OH}]_0}\right) = -(k_5[\text{HNO}_3] + k_1[\text{NO}_2] + k_d) \cdot t = -k' \cdot t \quad (\text{ii})$$

where [OH]₀ and [OH]_t are the initial and time dependent [OH] concentrations (proportional to the OH-LIF signal), respectively. The pseudo first-order rate coefficient k' comprises the rate coefficients for the target reaction HNO₃ with OH (k_5), the reaction between NO₂ and OH (k_1) and diffusion out of the reaction zone (k_d). A typical series of OH-LIF profiles is illustrated in Fig. 5. The OH decay was found to be strictly mono-exponential, so that a pseudo-first order rate coefficient k' could be calculated from the slope of each curve. Values of k' were corrected for the term $k_1[\text{NO}_2]$ to yield k^{cor} and k_5 was obtained from the slopes of plots of k^{cor} versus [HNO₃] (Fig. 6). The intercept is due to transport and diffusion processes, i.e. k_d and was typically $\sim 100 \text{ s}^{-1}$ at $p = 20 \text{ Torr}$ and close to zero at $p > 200 \text{ Torr}$.

Altogether, more than eighty determination of k_5 were made at various temperatures and pressures, in N₂ and air bath gases and using three different HNO₃ sources. Neither the source of HNO₃ nor the identity of the bath gas had a measurable influence on the rate coefficients obtained. Due to efficient quenching of OH fluorescence by O₂, most measurements were conducted in nitrogen bath gas instead of synthetic air to optimise the signal quality. Rate coefficients obtained in air (at 275 and 297 K) agreed within 4% with those obtained in N₂, which is consistent with the results of earlier studies (Stachnik et al., 1986; Brown et al., 1999).

The temperature and pressure inside the photolysis cell were varied over as large a range as possible (208 – 318 K and 18–696 Torr), with the lower temperature limit determined by HNO₃ condensation. At temperatures lower than 208 K, large fluctuations in the measured optical density of HNO₃ were evidence of strong partitioning to the walls of the reactor, with periodic modulation of gas-phase [HNO₃] arising via weak temperature cycling ($\pm 0.5 \text{ }^\circ\text{C}$) of the cryostat. The HNO₃ concentration changed by up to 50% during these experiments and gave rise to inaccurate kinetic data and scattered plots of k' versus [HNO₃]. For this reason we report no data below 208 K.

Our measurements reveal a strong temperature and pressure dependence of k_5 under some conditions. The rate coefficients obtained in N₂ are summarised in Fig. 7 and listed in Table S1 (supplementary information). Note that data of similar quality obtained at 239 and 246 K are not plotted in Fig. 7 to preserve clarity of presentation. The error bars (total uncertainty) include 2 σ statistical uncertainty as derived from fits to the data as in Fig. 3 and 4) and an estimate of systematic error. At



room temperature and for pressures up to ~ 300 Torr, the overall uncertainty in k_5 depends mainly on the $[\text{HNO}_3]$ measurements and we assign a value of 7% to cover both uncertainty in the cross sections at 214.86 and 184.95 nm and additional uncertainty due to slight drifts in measurement of optical density at 213.86 nm. At low temperatures, the total uncertainty increased as more HNO_3 was stored on the walls of the reactor (leading to periodic modulation of $[\text{HNO}_3]$) and due to the use of a restricted range of $[\text{HNO}_3]$ (to keep the condensation problem manageable). Thus at 208 K and 217 K a further 10% was added to the overall uncertainty, increasing it to $\approx 17\%$.

Over the range of temperature and pressure covered in these experiments, k_5 varied over a factor of ~ 6 . Although a positive trend in k_5 with bath gas pressure is evident at 297 and 276 K, the dependence is very weak and is only observable due to the high precision of the dataset. At temperatures of 257 K and below, the pressure dependence is more pronounced.

The temperature dependence of k_5 at two constant bath gas densities (8.9×10^{17} and 2.1×10^{19} molecule cm^{-3} , corresponding to pressures of ≈ 27 and ≈ 650 Torr, respectively) is illustrated in Fig. 8. The negative dependence of k_5 on temperature is very clear in both cases. The data at the lower pressure are reproduced by a simple Arrhenius expression: k_5 ($M = 8.88 \times 10^{17}$ molecule cm^{-3}) = $3.29 \times 10^{-15} \exp(1079/T)$ $\text{cm}^3 \text{ molecule}^{-1} \text{ s}^{-1}$. At the higher pressure curvature is more evident, though the expression k_5 ($[M] = 2.1 \times 10^{19}$ molecule cm^{-3}) = $2.29 \times 10^{-15} \exp(1221/T)$ $\text{cm}^3 \text{ molecule}^{-1} \text{ s}^{-1}$ captures most of the data points. Only at pressures much lower than those achievable with the present set-up does the temperature dependence show a significant change in the apparent (negative) activation energy with e.g. a value of $k_5 = 2 \times 10^{-14} \exp(430/T)$ $\text{cm}^3 \text{ molecule}^{-1} \text{ s}^{-1}$ obtained in a few Torr of He (Connell and Howard, 1985).

The solid fit-lines in Fig. 7 were obtained by a least-squares fit to the present data-sets using the expression derived by (Lamb et al., 1984) and which has been used on several occasions for parameterising k_5 :

$$k_5 = k_0(T) + k_p(M, T) = k_0 + \frac{k_c[M]}{1 + k_c[M]/k_\Delta} \quad (\text{iii})$$

Here, the overall rate coefficient, k_5 , is comprised of a pressure-independent rate coefficient $k_0(T) = A_0 \exp(E_0/T)$ and a Lindemann-Hinshelwood type term, $k_p(M, T)$, for the pressure dependence. $k_c = A_c \exp(E_c/T)$ is the termolecular rate coefficient for formation of the thermalised complex, $k_\Delta = A_\Delta \exp(E_\Delta/T)$ is $k_\infty - k_0$, the difference between the high- and low-pressure limiting rate coefficients (k_∞ and k_0 , respectively) and $[M]$ is the bath gas concentration. As our data do not define the rate coefficient close to the low-pressure limit, we guided the six-parameter fit (equation iii) by adding data points at $M = 2.5 \times 10^{16}$ molecule cm^{-3} calculated using $k_5 = 2 \times 10^{-14} \exp(430/T)$ $\text{cm}^3 \text{ molecule}^{-1} \text{ s}^{-1}$ from the low pressure study of Connell and Howard (1985). This is represented by the vertical, solid line in Fig. 7, which covers temperatures between 220 and 330 K. The low pressure dataset of Connell and Howard (1985) is more extensive and, due to the use of in-situ optical measurements of HNO_3 using the same cross section as derived here, is considered to be more accurate than others obtained at about the same time (Jourdain et al., 1982; Devolder et al., 1984). The rate coefficients of Connell and Howard were obtained in He and thus assigned an equivalent pressure in N_2 using the relative collision efficiency (0.38) derived by Brown et al. (1999) However, in the low pressure regime, there is only a weak dependence of k_5 on pressure so that constraining the



fits with data obtained in He will not introduce significant error. Equation (iii) and the parameters listed in Table 1 clearly describe our entire dataset very well. We note that re-fitting the dataset after removing the data with the largest uncertainty (i.e. that at the lowest temperatures of 208 and 217 K) has the effect of slightly *increasing* the predicted rate coefficient at the lowest temperatures. This is in the opposite direction to that which would result from the potential systematic overestimation of HNO₃ concentrations at the centre of the reactor during the experiments at the lowest temperatures (see discussion in section 3.2).

3.5 Comparison with literature and parameterisation of k_5 for atmospheric modelling

In order to avoid a lengthy and repetitive discussion of previous literature results we restrict our comparison to datasets obtained in N₂ (or air) which are the most relevant for atmospheric chemistry. Apart from the present study we use data from Jolly et al. (1985), Stachnik et al. (1986), Brown et al. (1999) and Carl et al. (2001). We have corrected the data of Stachnik et al. (1986) (divided each rate coefficient by 1.13) to take into account their use of absorption cross sections (Molina and Molina, 1981) of HNO₃ at 195 and 200 nm that were ~ 13% larger than those reported subsequently (Burkholder et al., 1993) which were obtained by more accurate methods and which agree well with the present cross section at 213.86 nm. As there are no obvious reasons to exclude any data from the studies listed above, we have performed a global fit to the complete set of 142 separate determinations of k_5 in N₂ / air covering pressures of ≈ 20 -700 Torr and temperatures of 200 to 350 K. These studies were all conducted at pressures of N₂ of >15 Torr and do not define the rate constant well at low pressures. As described above for analysis of the present dataset, we have added rate coefficients at low pressures based on the flow tube experiments of Connell and Howard (1985) to guide the fit towards the experimental values obtained at pressures close to the low-pressure limit.

Figure 9 provides an overview of experimental room temperature rate coefficients determined in N₂ bath-gas by different groups. The plot also shows the parameterised rate coefficient (using the values listed in the lower part of Table 1) obtained by fitting to all datasets at all temperatures and pressures (solid line). The results are in good agreement and even the “outliers” (Jolly et al., 1985; Carl et al., 2001) agree to within 15% with the parameterisation.

In Fig. 10, we compare temperature dependent values of k_5 from the parameterisation with literature data. The upper panel compares the results of the parameterisation to the present dataset, the lower panel compares it to the dataset of Brown et al. (1999) which, prior to the present data, represented the largest set of experimental rate coefficients available in the literature for N₂ bath gas. Figure 10 shows that the parameterisation reproduces most of the literature data obtained in N₂ bath gas, although the dataset of Brown et al. (1999), indicates a slightly stronger pressure dependence at most temperatures. The deviation between parameterisation and measurement is greatest for the higher temperature datasets (325, 350 K) of Brown et al. As atmospheric HNO₃ is not significantly removed by reaction with OH at temperatures above ≈ 300 K, this does not represent a problem for use of this parameterisation for atmospheric modelling. At low temperatures (where loss of HNO₃ by reaction with OH is most important) the parameters capture the pressure and temperature dependence reasonably well.



Figure 11 displays the ratio of the values of k_5 calculated from the parameterisation presented in the present study to that derived by the IUPAC (Atkinson et al., 2004; IUPAC, 2017) and NASA-JPL (Burkholder et al., 2016) assessments, which adopted the parameters suggested by Brown et al. (1999). At pressures (< 200 mbar) and temperatures (< 240 K) typically associated with the upper troposphere and lower stratosphere, the new parameterisation results in lower values of k_5 with a decrease in k_5 of up to 20% at 180 K. The new parameterisation reduces k_5 by up to 10% for the warmer (> -10 °C) temperatures associated with the lowermost troposphere.

3.5 Global impact of new parameterisation of k_5

The atmospheric impact of the new parameterisation of k_5 will depend on other chemical processes that generate, remove and interconvert HNO_3 and NO_x including photolysis and deposition of HNO_3 , reaction of NO_2 with OH, the heterogeneous loss of N_2O_5 as well as vertical and horizontal transport and was therefore examined using a global atmospheric model. We investigated the differences in model predictions of HNO_3 and NO_x mixing ratios which resulted from switching from the presently recommended parameterisation (Atkinson et al., 2004; Burkholder et al., 2016) based on the data of Brown et al. (1999) to that presented in this manuscript. The EMAC (ECHAM/MESSy Atmospheric Chemistry) model employed for this analysis is a numerical chemistry and climate simulation system (Jöckel et al., 2006; Jöckel et al., 2010) using the 5th generation European Centre Hamburg general circulation model (ECHAM5, Roeckner et al. (2006)) as core atmospheric general circulation model. For the present study we applied EMAC (ECHAM5 version 5.3.02, MESSy version 2.53.0) in the T42L47MA-resolution, i.e. with a spherical truncation of T42 (corresponding to a quadratic Gaussian grid of approx. 2.8 by 2.8 degrees in latitude and longitude) with 47 vertical hybrid pressure levels up to 0.01 hPa. The model has been weakly nudged in spectral space, nudging temperature, vorticity, divergence and surface pressure (Jeuken et al., 1996). The chemical mechanism scheme adopted (MOM, Mainz Organic Mechanism) includes oxidation of isoprene, saturated and unsaturated hydrocarbons, including terpenes and aromatics (Cabrera-Perez et al., 2016; Lelieveld et al., 2016). Further, tracer emissions and model set-up are similar to the one presented in Lelieveld et al. (2016). EMAC model predictions have been evaluated against observations on several occasions (Pozzer et al., 2010; de Meij et al., 2012; Yoon and Pozzer, 2014): For additional references, see <http://www.messy-interface.org>. For this study, EMAC was used in a chemical-transport model (CTM mode) (Deckert et al., 2011), i.e., by disabling feedbacks between photochemistry and dynamics. Two years were simulated (2009-2010), with the first year used as spin-up time. The lower panel of Fig. 11 illustrates the latitude and altitude dependent changes (zonal and annual averages) in the modelled rate coefficient k_5 . Increases in k_5 (up to 8%) are seen throughout the lower stratosphere, whereas the warmer temperatures and higher pressures of the troposphere generally result in a decrease in k_5 .

The results of the model simulations are expressed in Fig. 12 as percentage changes in the zonally and annual averaged HNO_3 (upper panel) and NO_x mixing ratios (lower panel) as a function of latitude and altitude. The largest relative changes in HNO_3 are found in the tropical upper troposphere (+ 4%) with a corresponding reduction in NO_x of 2%. The largest relative change in NO_x (+4%) is predicted to be in the lower stratosphere (18-23 km) at mid- and high-latitudes. As HNO_3



and NO_x are impacted in different directions by changing k_5 , the HNO₃ / NO_x ratio will be most strongly affected. The predicted, global relative change in the HNO₃ / NO_x ratio (Fig. S4 of the supplementary information) was found to be -6% in the tropical upper troposphere and +6% in the lower stratosphere. Given the importance of HNO₃ to NO_x partitioning in governing rates of photochemical ozone production, the impact of the changes in k_5 are significant.

5

4 Conclusions

We have obtained a large number of rate coefficients (k_5) for the reaction between OH and HNO₃, the associated uncertainty of which was minimised through in-situ optical measurements of HNO₃ by both absorption and fluorescence methods and detailed analysis of impurities. The pressure and temperature dependent rate coefficients confirm the results of an earlier study (Brown et al., 1999), which found a strong increase in the pressure dependence of k_5 at low temperatures. The rate coefficients were combined with previous results to give a global parameterisation that is applicable to the Earth's atmosphere and which results in latitude and altitude dependent changes in the HNO₃ / NO_x ratio of between +6 and -6%.

Acknowledgements

15 We thank the Deutsche Forschungsgemeinschaft (DFG) for partial financial support (CR 246/2-1). We are grateful to The Chemours Company (CH) for providing a sample of the FEP suspension used to coat the reactor.

References

- 20 Aloisio, S., and Francisco, J. S.: Structure and energetics of hydrogen bonded HO_x-HNO₃ complexes, *J. Phys. Chem. A*, 103, 6049-6053, 1999.
- Atkinson, R., Baulch, D. L., Cox, R. A., Crowley, J. N., Hampson, R. F., Hynes, R. G., Jenkin, M. E., Rossi, M. J., and Troe, J.: Evaluated kinetic and photochemical data for atmospheric chemistry: Volume I - gas phase reactions of O_x, HO_x, NO_x and SO_x species, *Atmos. Chem. Phys.*, 4, 1461-1738, 2004.
- 25 Biau, F.: Nitric acid vapour absorption cross-section spectrum and its photodissociation in the stratosphere, *J. Photochem.*, 2, 139-149, 1973-1974.
- Bogumil, K., Orphal, J., Homann, T., Voigt, S., Spietz, P., Fleischmann, O. C., Vogel, A., Hartmann, M., Kromminga, H., Bovensmann, H., Frerick, J., and Burrows, J. P.: Measurements of molecular absorption spectra with the SCIAMACHY pre-flight model: instrument characterization and reference data for atmospheric remote-sensing in the 230-2380 nm region, *J. Photochem. Photobiol. A-Chem.*, 157, 167-184, doi:10.1016/s1010-6030(03)00062-5, 2003.
- 30 Brown, S. S., Talukdar, R. K., and Ravishankara, A. R.: Reconsideration of the rate constant for the reaction of hydroxyl radicals with nitric acid, *J. Phys. Chem.*, 103, 3031-3037, 1999.



- Brown, S. S., Burkholder, J. B., Talukdar, R. K., and Ravishankara, A. R.: Reaction of hydroxyl radical with nitric acid: Insights into its mechanism, *J. Phys. Chem.*, 105, 1605-1614, 2001.
- Burkholder, J. B., Talukdar, R. K., Ravishankara, A. R., and Solomon, S.: Temperature dependence of the HNO₃ UV absorption cross-sections, *J. Geophys. Res. -Atmos.*, 98, 22937-22948, 1993.
- 5 Burkholder, J. B., Sander, S. P., Abbatt, J., Barker, J. R., Huie, R. E., Kolb, C. E., Kurylo, M. J., Orkin, V. L., Wilmouth, D. M., and Wine, P. H.: Chemical Kinetics and Photochemical Data for Use in Atmospheric Studies, Evaluation No. 18," JPL Publication 15-10, Jet Propulsion Laboratory, Pasadena, <http://jpldataeval.jpl.nasa.gov>, 2016.
- Butkovskaya, N., Kukui, A., and Le Bras, G.: HNO₃ forming channel of the HO₂+NO reaction as a function of pressure and temperature in the ranges of 72-600 torr and 223-323 K, *J. Phys. Chem. A*, 111, 9047-9053, 2007.
- 10 Butkovskaya, N., Rayez, M. T., Rayez, J. C., Kukui, A., and Le Bras, G.: Water Vapor Effect on the HNO₃ Yield in the HO₂ + NO Reaction: Experimental and Theoretical Evidence, *J. Phys. Chem. A*, 113, 11327-11342, doi:10.1021/jp811428p, 2009.
- Cabrera-Perez, D., Taraborrelli, D., Sander, R., and Pozzer, A.: Global atmospheric budget of simple monocyclic aromatic compounds, *Atmos. Chem. Phys.*, 16, 6931-6947, 2016.
- Cariolle, D., Evans, M. J., Chipperfield, M. P., Butkovskaya, N., Kukui, A., and Le Bras, G.: Impact of the new HNO₃-forming channel of the HO₂+NO reaction on tropospheric HNO₃, NO_x, HO_x and ozone, *Atmos. Chem. Phys.*, 8, 4061-4068, 2008.
- 15 Carl, S. A., Ingham, T., Moortgat, G. K., and Crowley, J. N.: OH kinetics and photochemistry of HNO₃ in the presence of water vapor, *Chem. Phys. Lett.*, 341, 93-98, 2001.
- Connell, P. S., and Howard, C. J.: Kinetics study of the reaction HO + HNO₃, *Int. J. Chem. Kinet.*, 17, 17-31, 1985.
- Crowley, J. N., Burrows, J. P., Moortgat, G. K., Poulet, G., and LeBras, G.: Optical detection of NO₃ and NO₂ in "pure" HNO₃ vapor, the liquid-phase decomposition of HNO₃, *Int. J. Chem. Kinet.*, 25, 795-803, 1993.
- 20 de Meij, A., Pozzer, A., Pringle, K. J., Tost, H., and Lelieveld, J.: EMAC model evaluation and analysis of atmospheric aerosol properties and distribution with a focus on the Mediterranean region, *Atmospheric Research*, 114, 38-69, 2012.
- Deckert, R., Jockel, P., Grewe, V., Gottschaldt, K. D., and Hoor, P.: A quasi chemistry-transport model mode for EMAC, *Geoscientific Model Development*, 4, 195-206, 2011.
- 25 Devolder, P., Carlier, M., Pauwels, J. F., and Sochet, L. R.: Rate constant for the reaction of OH with nitric acid, *Chem. Phys. Lett.*, 111, 94-99, 1984.
- Gonzalez, J., and Anglada, J. M.: Gas Phase Reaction of Nitric Acid with Hydroxyl Radical without and with Water. A Theoretical Investigation, *J. Phys. Chem. A*, 114, 9151-9162, doi:10.1021/jp102935d, 2010.
- IUPAC: Task Group on Atmospheric Chemical Kinetic Data Evaluation, (Ammann, M., Cox, R.A., Crowley, J.N., Herrmann, H., Jenkin, M.E., McNeill, V.F., Mellouki, A., Rossi, M. J., Troe, J. and Wallington, T. J.) <http://iupac.pole-ether.fr/index.html>, <http://iupac.pole-ether.fr/index.html>, 2017.
- 30 Jeuken, A. B. M., Siegmund, P. C., Heijboer, L. C., Feichter, J., and Bengtsson, L.: On the potential of assimilating meteorological analyses in a global climate model for the purpose of model validation, *J. Geophys. Res. -Atmos.*, 101, 16939-16950, 1996.
- Jöckel, P., Tost, H., Pozzer, A., Bruhl, C., Buchholz, J., Ganzeveld, L., Hoor, P., Kerkweg, A., Lawrence, M. G., Sander, R., Steil, B., Stiller, G., Tanarhte, M., Taraborrelli, D., Van Aardenne, J., and Lelieveld, J.: The atmospheric chemistry general circulation model ECHAM5/MESSy1: consistent simulation of ozone from the surface to the mesosphere, *Atmos. Chem. Phys.*, 6, 5067-5104, 2006.
- Jöckel, P., Kerkweg, A., Pozzer, A., Sander, R., Tost, H., Riede, H., Baumgaertner, A., Gromov, S., and Kern, B.: Development cycle 2 of the Modular Earth Submodel System (MESSy2), *Geoscientific Model Development*, 3, 717-752, 2010.



- Jolly, G. S., Paraskevopoulos, G., and Singleton, D. L.: The question of a pressure effect in the reaction OH + HNO₃. A laser flash-photolysis resonance-absorption study, *CPL*, 117, 132-137, 1985.
- Jourdain, J. L., Poulet, G., and Le Bras, G.: Determination of the rate parameters and products for the reaction of hydroxyl radicals with nitric acid, *J. Chem. Phys.*, 76, 5827-5833, 1982.
- 5 Kenner, R. D., Rohrer, F., and Stuhl, F.: Determination of the Excitation Mechanism for Photofragment Emission in the ArF Laser Photolysis of NH₃, N₂H₄, HNO₃ and CH₃NH₂, *Chem. Phys. Lett.*, 116, 374-379, 1985.
- Kenner, R. D., Rohrer, F., Papenbrock, T., and Stuhl, F.: Excitation mechanism for OH(A) in the ArF excimer laser photolysis of nitric acid *J. Phys. Chem.*, 90, 1294-1299, doi:10.1021/j100398a018, 1986.
- Kurylo, M. J., Cornett, K. D., and Murphy, J. L.: The Temperature-Dependence of the Rate-Constant For the Reaction of Hydroxyl
- 10 Radicals With Nitric-Acid, *J. Geophys. Res. -Atmos.*, 87, 3081-3085, 1982.
- Lamb, J. J., Mozurkewich, M., and Benson, S. W.: Negative activation energies and curved Arrhenius plots 3. OH + HNO₃ AND OH + HNO₄, *J. Phys. Chem.*, 88, 6441-6448, 1984.
- Lelieveld, J., Gromov, S., Pozzer, A., and Taraborrelli, D.: Global tropospheric hydroxyl distribution, budget and reactivity, *Atmos. Chem. Phys.*, 16, 12477-12493, 2016.
- 15 Margitan, J. J., Kaufman, F., and Anderson, J. G.: Kinetics of reaction OH + HNO₃ -> H₂O + NO₃, *Int. J. Chem. Kinet.*, 1, 281-287, 1975.
- Margitan, J. J., and Watson, R. T.: Kinetics of the Reaction of Hydroxyl Radicals With Nitric-Acid, *J. Phys. Chem.*, 86, 3819-3824, 1982.
- Marinelli, W. J., and Johnston, H. S.: Reaction-Rates of Hydroxyl Radical With Nitric-Acid and With Hydrogen-Peroxide, *J. Chem. Phys.*, 77, 1225-1234, 1982.
- McCabe, D. C., Brown, S. S., Gilles, M. K., Talukdar, R. K., Smith, I. W. M., and Ravishankara, A. R.: Kinetics of the removal of
- 20 OH(v=1) and OD(v= 1) by HNO₃ and DNO₃ from 253 to 383 K, *J. Phys. Chem. A*, 107, 7762-7769, 2003.
- Molina, L. T., and Molina, M. J.: Uv Absorption Cross-Sections of Ho2no2 Vapor, *J. Photochem.*, 15, 97-108, 1981.
- O'Donnell, B. A., Li, E. X. J., Lester, M. I., and Francisco, J. S.: Spectroscopic identification and stability of the intermediate in the OH+HONO₂ reaction, *Proc. Natl. Acad. Sci. U. S. A.*, 105, 12678-12683, doi:10.1073/pnas.0800320105, 2008a.
- O'Donnell, B. A., Li, E. X. J., Lester, M. I., and Francisco, J. S.: Spectroscopic identificationj and stability of the intermediate in the OH +
- 25 HNO₃ reaction, *Proc. Natl. Acad. Sci. U.S.A*, 105, 12678-12683, 2008b.
- Papenbrock, T., Haak, H. K., and Stuhl, F.: ArF laser (193 nm) photolysis of HNO₃ - Formation of excited fragments, *Berichte Der Bunsen-Gesellschaft-Physical Chemistry Chemical Physics*, 88, 675-679, 1984.
- Papenbrock, T., and Stuhl, F.: Measurement of gaseous nitric-acid by a laser-photolysis fragment-fluorescence (LPFF) method in the Black-Forest and at the North-Sea coast, *Atmos. Env. A*, 25, 2223-2228, doi:10.1016/0960-1686(91)90097-q, 1991.
- 30 Pozzer, A., Pollmann, J., Taraborrelli, D., Jockel, P., Helmig, D., Tans, P., Hueber, J., and Lelieveld, J.: Observed and simulated global distribution and budget of atmospheric C-2-C-5 alkanes, *Atmos. Chem. Phys.*, 10, 4403-4422, 2010.
- Ravishankara, A. R., Eisele, F. L., and Wine, P. H.: Study of the Reaction of Oh With Hno3 - Kinetics and No3 Yield, *J. Phys. Chem.*, 86, 1854-1858, 1982.
- Roeckner, E., Brokopf, R., Esch, M., Giorgetta, M., Hagemann, S., Kornblueh, L., Manzini, E., Schlese, U., and Schulzweida, U.:
- 35 Sensitivity of simulated climate to horizontal and vertical resolution in the ECHAM5 atmosphere model, *Journal of Climate*, 19, 3771-3791, 2006.



- Sander, S. P., Friedl, R. R., Golden, D. M., Kurylo, M. J., Moortgat, G. K., Keller-Rudek, H., Wine, P. H., Ravishankara, A. R., Kolb, C. E., Molina, M. J., Finlayson-Pitts, B. J., Huie, R. E., and Orkin, V. L.: Chemical kinetics and photochemical data for use in atmospheric studies: Evaluation Number 15, Jet Propulsion Laboratory, National Aeronautics and Space Administration / Jet Propulsion Laboratory / California Institute of Technology, Pasadena, CA, 2006.
- 5 Schultz, M. G., Jacob, D. J., Bradshaw, J. D., Sandholm, S. T., Dibb, J. E., Talbot, R. W., and Singh, H. B.: Chemical NO_x budget in the upper troposphere over the tropical South Pacific, *J. Geophys. Res. -Atmos.*, 105, 6669-6679, 2000.
- Smith, C. A., Molina, L. T., Lamb, J. J., and Molina, M. J.: Kinetics of the reaction of OH with pernitric and nitric acids, *Int. J. Chem. Kinet.*, 16, 41-55, 1984.
- Smith, I. W. M., and Zellner, R.: Rate measurements of OH by resonance-absorption.4. Reactions of OH with NH₃ and HNO₃, *Int. J. Chem. Kinet.*, 1, 341-351, 1975.
- 10 Stachnik, R. A., Molina, L. T., and Molina, M. J.: Pressure and temperature dependences of the reaction of OH with nitric-acid, *J. Phys. Chem.*, 90, 2777-2780, 1986.
- Staudt, A. C., Jacob, D. J., Ravetta, F., Logan, J. A., Bachiochi, D., Krishnamurti, T. N., Sandholm, S., Ridley, B., Singh, H. B., and Talbot, B.: Sources and chemistry of nitrogen oxides over the tropical Pacific, *J. Geophys. Res. -Atmos.*, 108, 2003.
- 15 Thakur, A. N., Singh, H. B., Mariani, P., Chen, Y., Wang, Y., Jacob, D. J., Brasseur, G., Müller, J.-F., and Lawrence, M.: Distribution of reactive nitrogen species in the remote free troposphere: data and model comparisons, *Atmos. Environ.*, 33, 1403-1422, 1999.
- Wine, P. H., Ravishankara, A. R., Kreutter, N. M., Shah, R. C., Nicovich, J. M., Thompson, R. L., and Wuebbles, D. J.: Rate of reaction of OH with HNO₃, *J. Geophys. Res. -Atmos.*, 86, 1105-1112, 1981.
- Wollenhaupt, M., Carl, S. A., Horowitz, A., and Crowley, J. N.: Rate coefficients for reaction of OH with acetone between 202 and 395 K, *J. Phys. Chem.*, 104, 2695-2705, 2000.
- 20 Xia, W. S., and Lin, M. C.: A multifacet mechanism for the OH+HNO₃ reaction: An ab initio molecular orbital/statistical theory study, *J. Chem. Phys.*, 114, 4522-4532, 2001.
- Yoon, J., and Pozzer, A.: Model-simulated trend of surface carbon monoxide for the 2001-2010 decade, *Atmos. Chem. Phys.*, 14, 10465-10482, 2014.

**Table 1.** Parameters for calculation of k_5 using equation (iii)

	Present dataset (in N ₂) plus parameterisation ^a of low pressure data
k_0	$1.58 \times 10^{-14} \exp(451/T) \text{ cm}^3 \text{ molecule}^{-1} \text{ s}^{-1}$
k_Δ	$1.23 \times 10^{-16} \exp(1854/T) \text{ cm}^3 \text{ molecule}^{-1} \text{ s}^{-1}$
k_c	$8.46 \times 10^{-32} \exp(525/T) \text{ cm}^6 \text{ molecule}^{-2} \text{ s}^{-1}$
	All data in N ₂ bath gas ^b plus parameterisation ^a of low P data
k_0	$1.32 \times 10^{-14} \exp(527/T) \text{ cm}^3 \text{ molecule}^{-1} \text{ s}^{-1}$
k_Δ	$9.73 \times 10^{-17} \exp(1910/T) \text{ cm}^3 \text{ molecule}^{-1} \text{ s}^{-1}$
k_c	$7.39 \times 10^{-32} \exp(453/T) \text{ cm}^6 \text{ molecule}^{-2} \text{ s}^{-1}$

^a $k_5 = 2 \times 10^{-14} \exp(430/T) \text{ cm}^3 \text{ molecule}^{-1} \text{ s}^{-1}$ at $M = 2.5 \times 10^{16} \text{ molecule cm}^{-3}$.^b140 data points in N₂ including this work, Stachnik et al. (1986) and Brown et al. (1999).

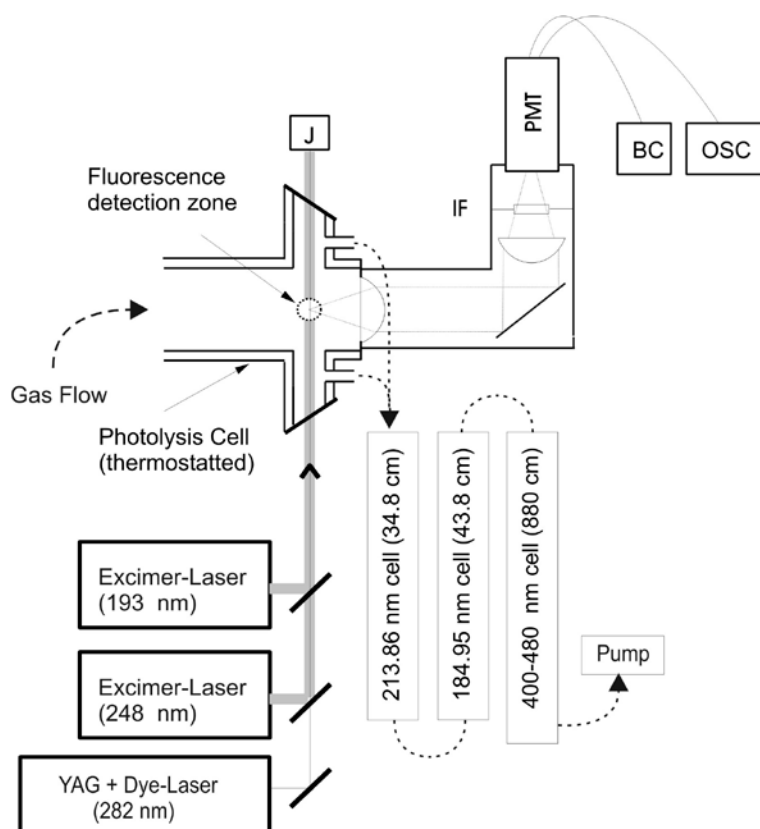


Figure 1: PLP-LIF setup. MFC = mass flow controller, PMT = photomultiplier tube, J = Joule meter, BC = box-car data acquisition, OSC = oscilloscope, IF = interference filter (309 ± 5 nm). Capacitance manometers monitored the pressure inside the reactor and the three optical absorption cells.



5

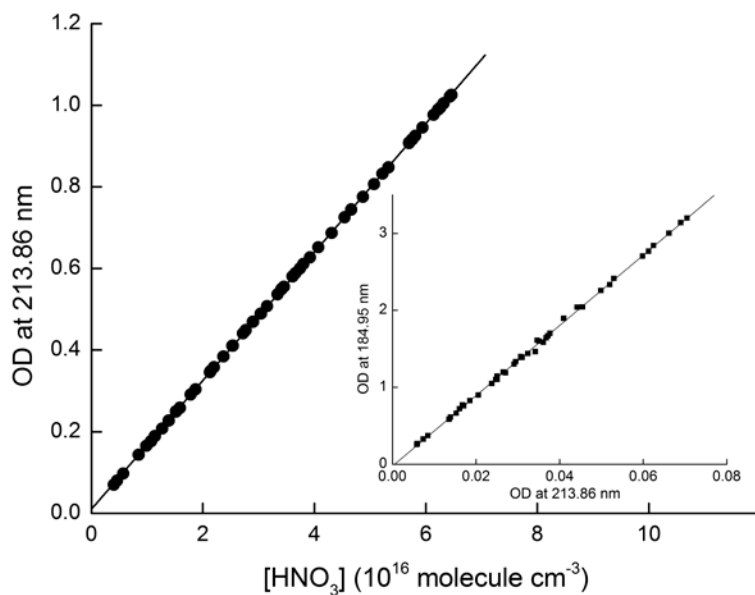


Figure 2: Beer-Lambert plot used for the calculation of the HNO₃ absorption cross section at 213.86 nm, $\sigma_{213.86 \text{ nm}}$. The inset shows the linear relation between optical densities (OD) at 184.95 nm and 213.86 nm.

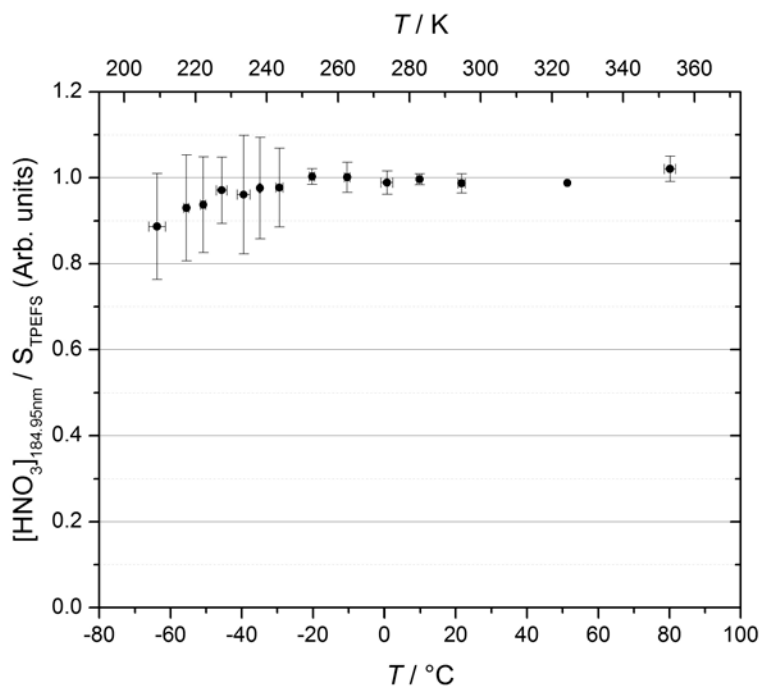


Figure 3. TPEFS detection of HNO₃ in the center of the reactor at different temperatures. The TPEFS signal (S_{TPEFS}) has been normalised to the HNO₃ concentration. The error bars indicate uncertainty derived from correction to the TPEFS signal due to quenching of fluorescence and absorption by HNO₃.

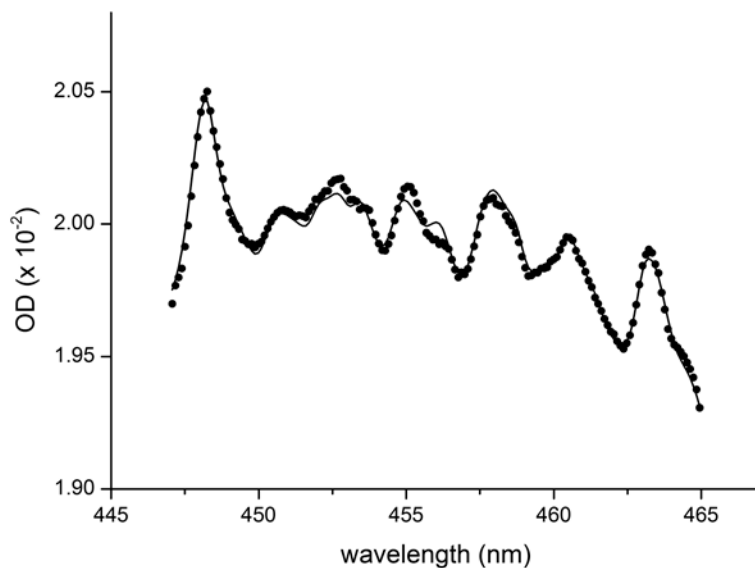


Figure 4. NO₂ impurity measurement (experiment at 298 K, 18 Torr) using the ternary mixture. The dotted line is the experimental NO₂ optical density (OD); the solid line is the fitted optical density using a reference spectrum (Bogumil et al., 2003). In this measurement, the NO₂ impurity corresponded to 0.01% of the HNO₃ concentration.

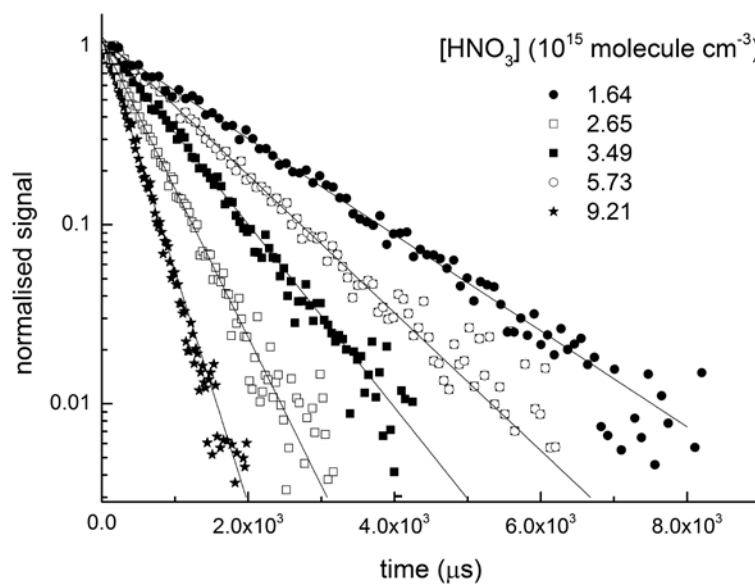


Figure 5. Temporal decay of the OH-LIF signal at 242 K and 50 Torr N_2 .

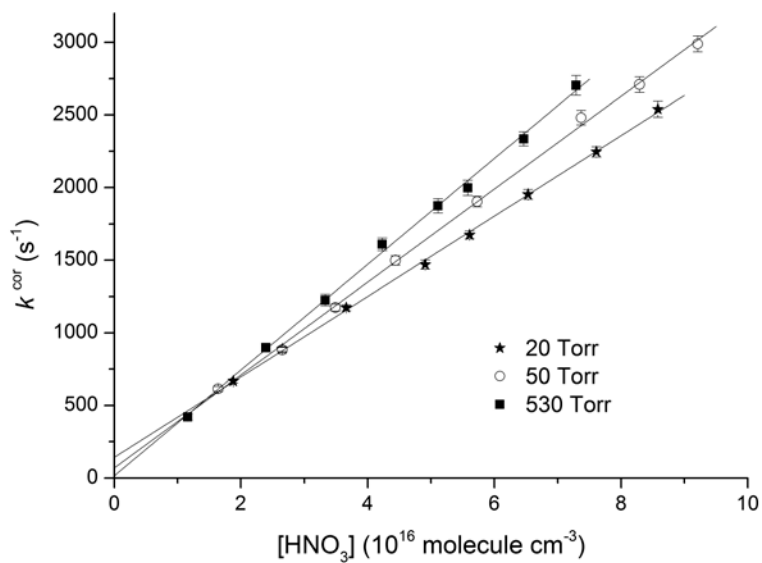


Figure 6. Corrected pseudo-first-order rate coefficients, k^{cor} , plotted as a function of the HNO_3 concentration. The data were obtained at 242 K and at three different pressures.

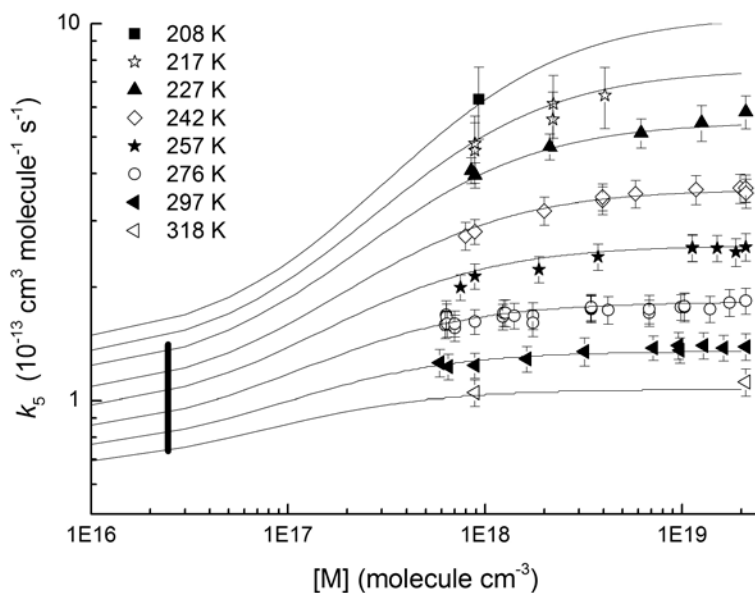


Figure 7. Rate coefficients k_5 as a function of pressure and temperature from this work (error bars represent total uncertainty). The solid lines are fits to the entire dataset with expression (iii). Data at 246 and 239 K are omitted to preserve clarity of presentation. The vertical line at $[M] = 2.5 \times 10^{16}$ molecule cm^{-3} (220–330 K) represents the dataset used to guide the fit at low pressures and is given by the expression $k_5 = 2 \times 10^{-14} \exp(430/T)$ $\text{cm}^3 \text{ molecule}^{-1} \text{ s}^{-1}$.

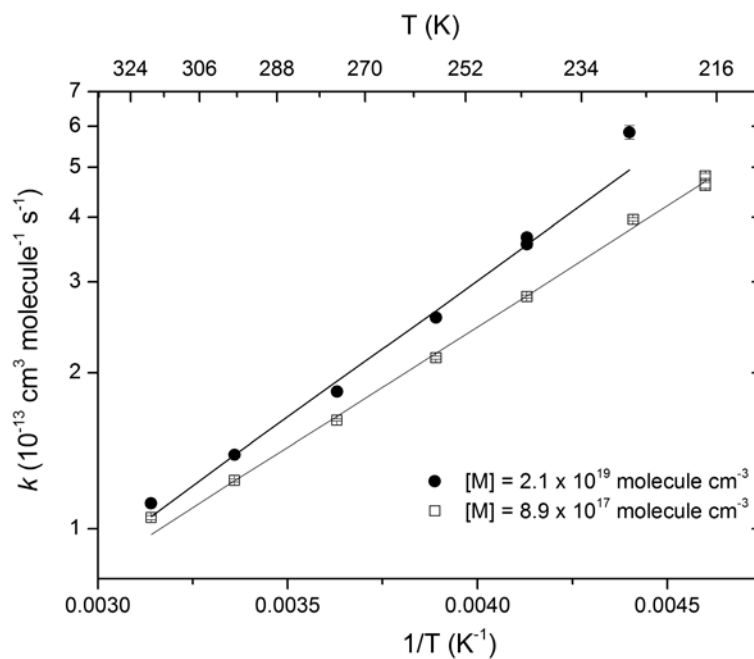


Figure 8. Temperature dependent rate coefficients at two constant bath gas concentrations $[M]$. The statistical uncertainties of the experimental data are within the symbol size. The solid lines are Arrhenius fits to the data (see text).

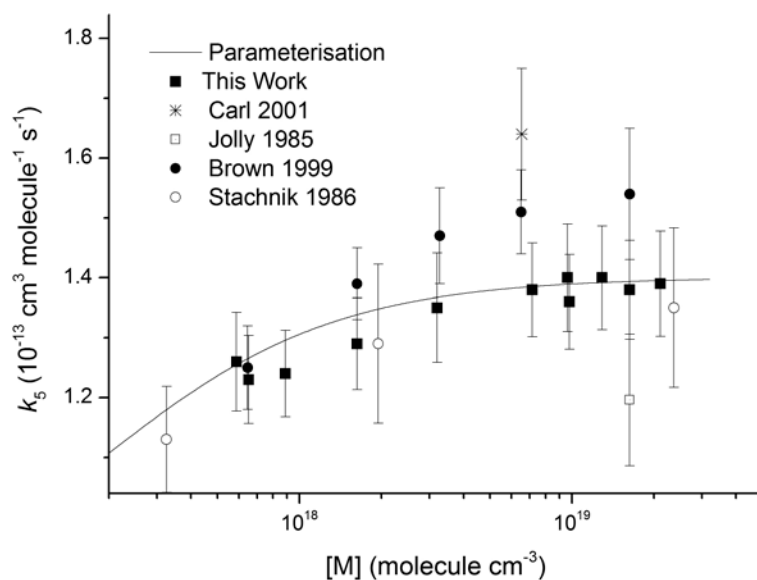


Figure 9. Comparison of room temperature rate coefficients (k_5) obtained in nitrogen bath gas. The error bars on our data points represent total uncertainty. The solid line are values of k_5 at 297 K from the parametrization obtained by fitting to the temperature and pressure dependent datasets from Brown et al. (1999), Stachnik et al. (1986), and this work.

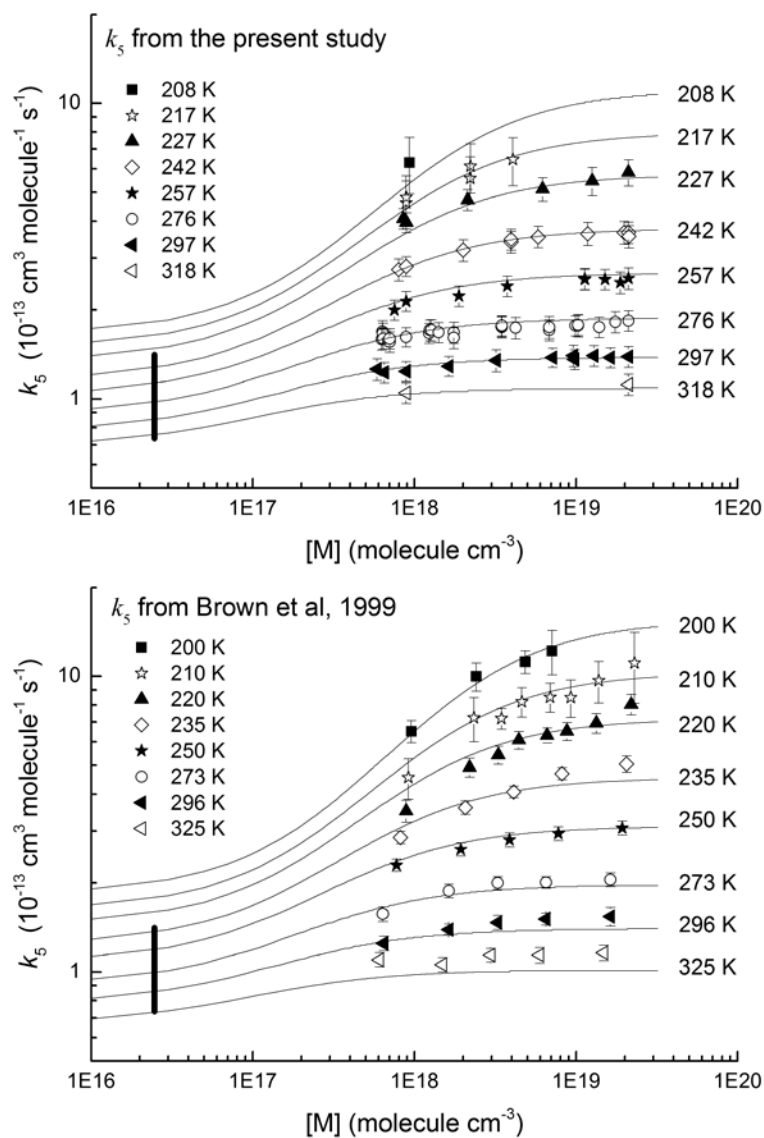


Figure 10. Rate coefficients k_5 as a function of pressure and temperature from Brown et al. (1999) (lower panel) and the present study (upper panel, error bars represent total uncertainty). The solid lines were derived from the parameters listed in Table 1 (lower panel). The vertical line at $M = 2.5 \times 10^{16}$ molecule cm^{-3} (220–330 K) represents the dataset used to constrain the fit at low pressures and is given by the expression $k_5 = 2 \times 10^{-14} \exp(430/T)$ $\text{cm}^3 \text{ molecule}^{-1} \text{ s}^{-1}$.

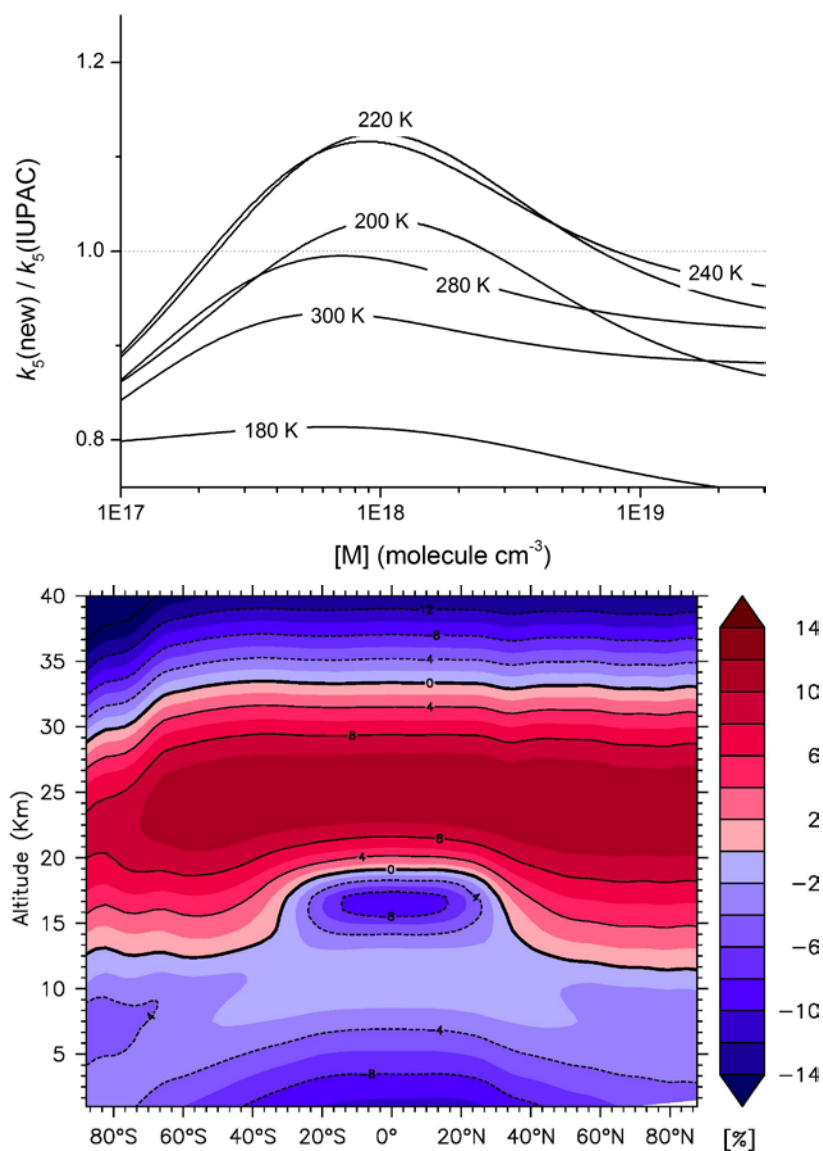


Figure 11. Upper panel: Ratio of rate coefficients obtained by combining results from this work with selected datasets from the literature, $k_5(\text{new})$, to those presently recommended by IUPAC, $k_5(\text{IUPAC})$. Lower panel: percentage change in rate coefficient k_5 calculated using annually and zonally averaged temperatures and pressure in the EMAC model.

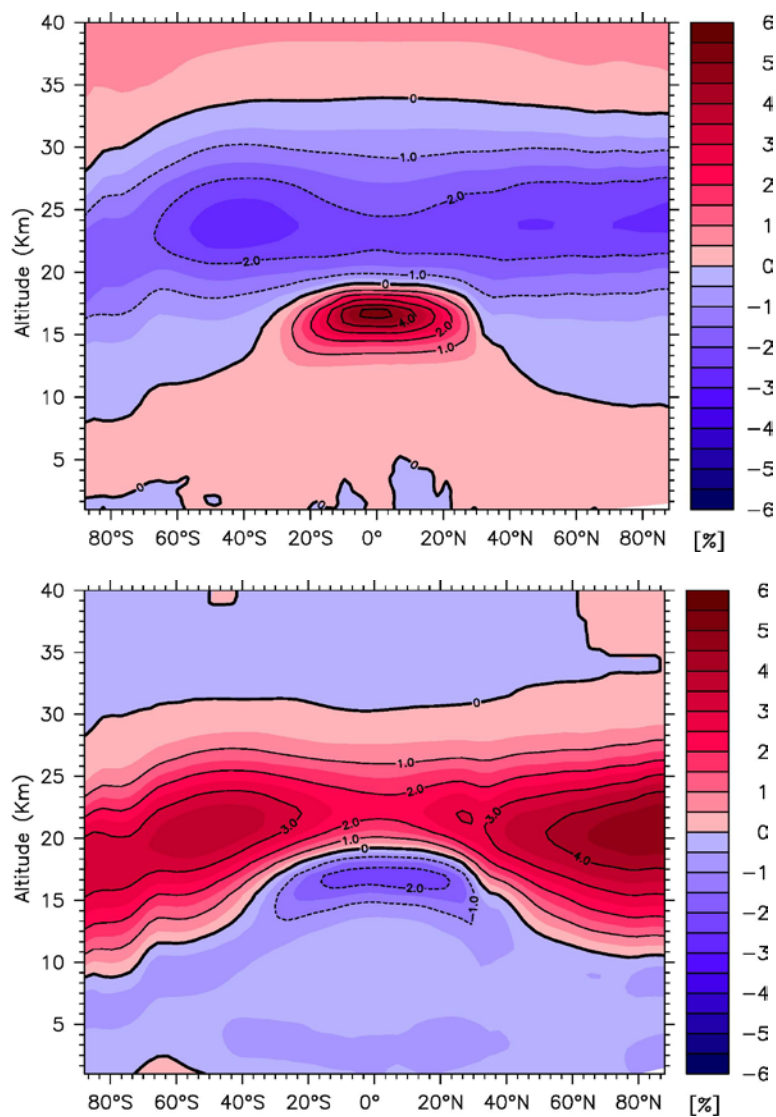


Figure 12. Impact of the results from this work in a global atmospheric chemistry model (EMAC). The contours indicate the percentage change in the predicted mixing ratios (zonal and annual average) of HNO₃ (upper panel) and NO_x (lower panel), which result from the new parameterization of k_5 .